Journal of Power Sources 450 (2020) 227581

Contents lists available at ScienceDirect

Journal of Power Sources

journal homepage: www.elsevier.com/locate/jpowsour

Fabrication of high-performance gas-diffusion-electrode based membrane-electrode assemblies

Scott A. Mauger [a,*], Jason R. Pfeilsticker [a], Min Wang [a], Samantha Medina [b], A. C. Yang-Neyerlin [a,b], K.C. Neyerlin [a], Caleb Stetson [b], Svitlana Pylypenko [a,b], Michael Ulsh [a]

[a] Chemistry and Nanoscience Center, National Renewable Energy Laboratory, Golden, CO, 80401, USA
[b] Department of Chemistry, Colorado School of Mines, Golden, CO, 80401, USA

HIGHLIGHTS

- Goal was to fabricate high-performance gas-diffusion-electrode-based fuel cells.
- The role of an ionomer overlayer and hot pressing were investigated.
- Both are critical for high performance.
- The overlayer and hot pressing reduce catalyst layer protonic resistance.
- There is a critical ionomer overlayer loading for maximum performance.

ARTICLE INFO

Keywords:
Gas diffusion electrodes
Membrane electrode assembly
Fuel cells
Fabrication

ABSTRACT

This work demonstrates the fabrication and processing steps required to produce high performance fuel cell membrane electrode assemblies (MEAs) based on spray-coated gas-diffusion electrodes (GDEs). It is demonstrated that coating the catalyst layer with a thin layer of ionomer and then hot pressing the GDEs to the membrane is required to achieve comparable catalyst activity and air performance to catalyst-coated-membrane MEAs. We show that there is a critical amount of ionomer required to achieve maximized performance. Using electron microscopy, we show that the combination of the ionomer overlayer and hot-pressing bonds the catalyst layer to the membrane, increasing the interfacial contact area and quality of this interface. We also find that the ionomer overlayer smooths the surface of the GDE and provides increased contact area between the GDE and the membrane. Additionally, we demonstrate that much less ionomer is required for high-performance than has been previously reported. Through model fitting of electrochemical impedance spectroscopy, we show that this improvement in the catalyst layer – membrane interface reduces the effective catalyst layer resistance, which reduces Ohmic losses and increases catalyst utilization.

1. Introduction

In polymer electrolyte fuel cell power systems, the membrane electrode assembly (MEA) is the critical component for power production as it is responsible for the electrochemical reactions that convert the fuel to power. While high performance materials (catalysts, membranes, and ionomers) are critical to achieving high-performance MEAs, the proper fabrication of these MEAs is also of great importance. Thus, there are many papers exploring the influences of different fabrication conditions such as catalyst ink formulation [1–6] and drying [2,7–12].

Another important consideration is how the MEA is constructed, as different MEA architectures have been shown to greatly influence fuel cell performance [10,13–20]. Catalyst layers can be applied directly to other MEA components or to a decal substrate that is used to transfer the catalyst layer. Direct coating is advantageous for manufacturing as it reduces processing steps – decreasing time and material waste. The two most common MEA architectures are the catalyst-coated membrane (CCM) and the gas-diffusion electrode (GDE), also sometimes referred to as a catalyst-coated diffusion media (CCDM) electrode. In a direct-coated CCM MEA, the catalyst layer is applied directly to the membrane. The gas diffusion media (GDM) can be hot pressed to the CCM MEA prior to assembly of the cell hardware. Or, without hot

* Corresponding author.
E-mail address: scott.mauger@nrel.gov (S.A. Mauger).

https://doi.org/10.1016/j.jpowsour.2019.227581
Received 8 October 2019; Received in revised form 2 December 2019; Accepted 6 December 2019
Available online 29 January 2020

pressing, the cell hardware can be used to press the GDMs to the MEA, with both methods resulting in good fuel cell performance. An advantage of CCMs is that coating the catalyst layer directly onto the membrane results in low contact resistance between the membrane and the catalyst layer [21,22]. In a GDE-based MEA the catalyst layer is applied to the microporous layer (MPL) of the GDM, which is generally hot pressed to the membrane to form the MEA [11,23,24]. Prior to the use of MPLs, GDEs suffered from low catalyst utilization because some catalyst was lost in the pores of the carbon paper and not electrochemically accessible [13].

GDEs are of interest for MEA fabrication because under some fabrication and/or operating conditions GDE MEAs have shown improved performance over CCM MEAs [14]. Some of these performance may be due to a better interface between the catalyst layer and MPL [25]. A poor interface between the MPL and catalyst layer may lead to increased electronic resistances and water pooling, which will limit reactant transport [1,3]. GDEs may also have advantages for roll-to-roll manufacturing due to more robust mechanical properties of the diffusion media and avoidance of membrane swelling during catalyst layer coating.

The challenge with GDEs is that the catalyst layer – membrane interface is usually inferior to that of CCMs, leading to lower performance. To overcome this, researchers have shown that coating a thin layer of ionomer on the catalyst layer improves this interface and thus fuel cell performance [2,8,10–12,26]. However, in a recent study focusing on the loading of this ionomer overlayer, the CCM MEAs out performed all GDE MEAs with an ionomer overlayer [10]. An alternative strategy recently developed is inkjet printing of a full membrane onto a GDEs to prepare MEAs, which have shown good performance [15–18]. There are also additional strategies, such catalyst layers with graded ionomer content and impregnated membranes, that have been employed to improve the catalyst layer/membrane interface and improve performance [27]. What is clear from all of these results is that a good catalyst layer/membrane interface is critical for high-performance fuel cells.

In this work we present a further comparative study of GDEs and CCMs and detail the fabrication conditions needed to achieve equivalent performance between CCM and GDE MEAs. We show that both an ionomer overlayer and hot pressing are required to achieve equivalent performance. Using electron and atomic force microscopy, we provide additional details of the mechanisms of performance enhancement due to the overlayer and show that it and hot pressing are required to achieve a good interface between the catalyst layer and the membrane. Finally, using electrochemical impedance spectroscopy (EIS) we analyze the effects of the overlayer and hot pressing on protonic resistance in the MEAs and show that the improved interface leads to a reduction in the catalyst layer proton resistance.

2. Experimental

2.1. Materials

For all catalyst layers (anode and cathode) a 47 wt% Pt on high surface area carbon (TKK TEC10E50E) was used as the catalyst material. A 20 wt% dispersion of Nafion in water and 1-propanol (Nafion D2020, 1000 EW, Ion Power) was used in preparation of the catalyst ink and Nafion overlayer ink. For all MEAs, the membrane was 25 μm thick Nafion (NR-211, 1100 EW, Ion Power). The diffusion media was Sigracet 29BC from SGL Carbon. Catalyst inks and Nafion overlayer inks were prepared using deionized water and 1-propanol.

2.2. Ink preparation

The catalyst layer inks were prepared by weighing the catalyst powder into a glass jar. To this jar deionized water was added (0.133 mL/mg Pt/HSC). After this addition, the jar was gently swirled to fully wet the catalyst powder. Next, 1-propanol was added (0.102 mL/mg Pt/HSC). Finally, the ionomer dispersion was added (2.37 μL/mg Pt/HSC) to achieve a 0.9 ionomer/carbon ratio by mass. To disperse the catalyst the jar was placed in a beaker filled with ice water. Next, the ink was tip sonicated for 10 s (QSonica Misonix S-400, 20 kHz, Amplitude = 1). The jar was then transferred to a bath sonicator, which was filled with ice water. The jar was sonicated for 20 min in four increments of 5 min each with gentle swirling between increments.

The ionomer dispersion for the overlayer was prepared by diluting the Nafion dispersion in water and 1-propanol. The ratios were 56 mL water/mL D2020 and 43 mL 1-propanol/mL D2020. This concentration of Nafion in this dispersion is the same as it was in the catalyst ink. The diluted dispersion was then stirred overnight.

2.3. Spray coating

The cathodes were prepared by spraying the catalyst ink directly to the diffusion media. Anodes were prepared by spraying the catalyst layer to the membrane. The inks were spray coated using a 25 kHz Accumist nozzle on a SonoTek ultrasonic spray coating station. The movement of the spray nozzle was controlled by Path Master software from SonoTek. The spray pattern was similar to that shown by Sassin et al. [21,28] with a full set of passes consisting of two horizontal and two vertical passes. The line spacing of the passes was 1.5 mm. For both sets of passes (horizontal and vertical) the second pass was offset from the first pass by 0.75 mm. The translational speed of the spray nozzle was 50 mm/s. There were no additional drying steps between passes as the catalyst layer was dry by the time nozzle reset to the starting position. For the catalyst layers the volumetric flow rate was 0.3 mL/min. For the ionomer overlayer the flow rate was 0.15 mL/min. The diffusion media and membranes were placed on a heated platen at 80 °C for spray coating. For the CCM anodes, the membrane was held in place by vacuum. During spray coating the catalyst and ionomer inks were continuously stirred to ensure a homogenous dispersion. The target loading for both the cathode and anode catalyst layers was 0.1 mg_{Pt}/cm^2.

2.4. Loading characterization

The loadings of the Pt/HSC catalyst layer and ionomer were varied by adjusting the number of spray coating passes. The Pt loadings of the GDEs were measured using energy dispersive x-ray fluorescence spectroscopy (Fischerscope XDV-SDD, 50 kV, 50 W x-ray source). For each GDE electrode the loading was measured at 5 locations to characterize the average loading. For all electrodes the Pt loading varied by less than 5% within the electrode. At a loading of 0.1 mg_{Pt}/cm^2 the measurement uncertainty of the instrument is less than 2%. Since the concentration of ionomer in the overspray ink was the same as the catalyst ink, the ionomer loading was estimated based on the expected Pt loading and defined I:C ratio.

2.5. MEA assembly

The MEAs were prepared by hot pressing the cathode GDE and anode diffusion media to the anode-coated membrane. The electrode area for both anode and cathode were 50 cm^2. The GDE/membrane/DM stacks were placed between two 5 inch by 5 inch sheets of Kapton. These were placed between two 4 inch by 4 inch sheets of 1/16 inch thick Gylon. These stacks were then placed between two 1/8 inch thick sheets of aluminum. Finally, these stacks were placed in a hydraulic press with heated plates (Carver) and pressed for 3 min at 125 °C. This temperature was selected based on previous studies which have shown that hot pressing at a temperature near Nafion's glass transition yields the best fuel cell performance [11,23,24]. The total applied force was 2500 kg. After pressing, the stacks were allowed to cool to near room temperature before the MEAs were removed from the aluminum plates and polymer sheets.

2.6. MEA testing

The MEAs were assembled into the testing hardware with graphite flow fields with double/triple (anode/cathode) serpentine patterns. The MEAs were sealed between PTFE gaskets. When fully assembled the diffusion media thickness was compressed to 75% of its original thickness assuming no compression of the membrane or catalyst layers. The MEAs were pre-conditioned with an initial voltage cycling break-in procedure and cycles of holding at 0.1 V followed by polarization curves [29,30]. This break-in and conditioning procedure has been shown to maximize catalytic activity and fuel cell performance. Polarization curves were measured at 80 °C, 100 %RH, 150 kPa absolute with an anodic sweep direction. The polarization curves reported were measured following the third conditioning cycle, based on prior work showing the mass activity plateaued after three cycles for this catalyst/membrane system [30]. O_2 polarization curves were measured with voltage-control mode. Air polarization curves were measured in current control mode with anode and cathode stoichiometries of 1.5 and 2, respectively. The cells were allowed to equilibrate at each potential/-current density for 3 min. The hydrogen-crossover current was measured 80 °C, 100% RH, 150 kPa with gas flows of 0.7 slpm/0.3 slpm H_2/N_2These values were used to for calculation of the oxygen-reduction reaction mass activity. The measured current density/potential is the average value measured in the 1 min following the equilibration period. Cyclic voltammograms (CVs) were measured at 30 °C, 150 kPa total cell pressure, 100 %RH, and H_2/N_2 respectively gas flows of at 0.50/0.05 slpm, respectively. The CVs were recorded from 0.05 to 1.2 V at a sweep rate of 50 mV/s using an Autolab potentiostat (MetrOhm). Electrochemical surface area (ECSA) was determined from the hydrogen underpotential deposition (H_{UPD}) region (≈0.08–0.4 V) of the CVs. EIS measurements were conducted at 80 °C, 150 kPa total cell pressure, 100 %RH, H_2/N_2 at 0.2/0.2 slpm, respectively. The spectra were measured at 40 points from 1 Hz–10 kHz on a logarithmic scale. The DC offset voltage was 0.2 V and the AC perturbation voltage was 1 mV. Standard deviations are reported based on measurements of multiple samples, which was three samples in most cases. More details of the conditioning and testing protocol can be found in Ref. 30.

2.7. Electrochemical impedance spectroscopy modeling

The EIS spectra were modeled using a custom programmed, open-source, complex-valued non-linear least-squares fitting program [31]. The program was written in Python using the SciPy package [32]. The model uses a physics based modified transmission line expression for the cell impedance developed by Setzler and Fuller, shown in Equation (1),

$$Z(\omega)_{model} = j\omega L_{wire} + R_{\Omega} + \sqrt{\frac{R_{CL}}{Q_{DL}(j\omega)^{\varphi}}}\coth\left(\sqrt{R_{CL}Q_{DL}(j\omega)^{\varphi}}\right). \quad (1)$$

where L_{wire} is cable inductance, R_{Ω} is ohmic resistance which is a combination of the membrane protonic resistance and cell (bulk and contact) electronic resistances [10,26], R_{CL} is the catalyst layer protonic sheet resistance (as defined by Neyerlin et al. [33]), Q_{DL} is the double layer constant phase element (CPE) parameter, and φ is the CPE exponent. The program fits the five parameters via the Levenberg–Marquardt algorithm with unity weighting [28].

The model can also be rewritten as in terms of a parameter array, $\boldsymbol{\beta}$.

$$Z(\boldsymbol{\beta},\omega)_{model} = j\omega\beta_1 + \beta_2 + \sqrt{\frac{\beta_3}{\beta_4(j\omega)^{\beta_5}}}\coth\left(\sqrt{\beta_3\beta_3(j\omega)^{\beta_5}}\right). \quad (2)$$

The cost function (Equation (3)) to be minimized during the fitting process was chosen to be the L2 norm (least squares) of the real and imaginary errors:

$$F_c(\boldsymbol{\beta}, Z(\omega)_{data}, \omega) = \sqrt{(Z'(\boldsymbol{\beta},\omega)_{model} - Z'(\omega)_{data})^2 + (Z''(\boldsymbol{\beta},\omega)_{model} - Z''(\omega)_{data})^2} \quad (3)$$

where $Z'(\boldsymbol{\beta},\omega)_{model}$ and $Z'(\omega)_{data}$ represent the real parts of the model and measured impedances, and $Z''(\boldsymbol{\beta},\omega)_{model}$ and $Z''(\omega)_{data}$ represent the real coefficients of the imaginary parts of the model and measured impedances. Standard final parameter error estimates (Equation (4)) were calculated as the square root of the diagonal elements of a first order estimated covariance matrix [28].

$$\sigma(\beta_i) \approx \sqrt{\frac{\boldsymbol{r}(\boldsymbol{\beta}^*)^T\boldsymbol{r}(\boldsymbol{\beta}^*)}{n-p}(\boldsymbol{J}^T\boldsymbol{J})^{-1}_{ii}} \quad (4)$$

Where i is the index of the desired parameter's standard deviation, $\boldsymbol{\beta}^*$ is the set of final parameters providing sufficiently minimal value for the cost function, $\boldsymbol{r}(\boldsymbol{\beta}^*)$ is the array of the final residuals at the input frequencies, $\boldsymbol{J}$ is the numerical Jacobian with respect to the parameters of the cost function evaluated at $\boldsymbol{\beta}^*$, n is the number of measurement points, and p is the number of parameters in the model.

2.8. Electron microscopy

In order to elucidate the cathode/membrane interfacial region for the various MEAs compared in this study both scanning electron microscopy (SEM) and transmission electron microscopy (TEM) were used. SEM cross-sectional views of the various MEAs were obtained by "freeze cutting" a portion of the MEA. A brand-new feather razor blade was used to swiftly cut the MEA on a glass slide after submerging the MEA in liquid nitrogen for approximately 30 s. The cross-sections were placed in the center of a mini vise specimen holder and imaged. Secondary electron (SE) images and backscattered electron (BSE) images were obtained with a JEOL 7000F FE-SEM operating at 10 kV accelerating voltage and 10 mm working distance.

Cross-sections for TEM analysis were obtained via ultramicrotomy. The samples were embedded in Araldite 6005 epoxy resin mixture, that was cured at 60 °C for 16 h, followed by block trimming and ultramicrotomy using a 36° clearance angle Diatome diamond knife. Bright field transmission electron microscopy (TEM) images were obtained in using a FEI Talos F200X electron microscope operated at 200 keV. The cross-sections were approximately 70 nm thick making them electron transparent for TEM.

2.9. AFM

AFM measurements were carried out using a Veeco Dimension 5000 system in tapping mode. Nanoscale surface roughness was imaged using Olympus AC160TS-R3 Si probes. Scan line density was 256 lines with 1024 samples/line. Nanoscale roughness was isolated from raw AFM images through second order polynomial flattening, thus reducing the tilt and bow associated with imaging of three-dimensional materials. After flattening, root mean square (RMS), or Rq, roughness was calculated to quantify datapoint height deviations from the mean height plane for the full images. Areas imaged in AFM were selected by navigating along the surfaces with the AFM instrument optical microscope, then imaging a representative region of the surface.

2.10. Surface profilometry

Micrometer-scale surface roughness measurements were conducted using a Veeco Dektak 8 Stylus Profilometer. The tip radius was 5 mm. The applied tip weight was 3 mg. The surface profile was recorded over a 3 mm scan length.

3. Results and discussion

In the following subsections we discuss the characteristics of the GDEs, the ionomer overlayer, and MEAs, including their physical properties. Next, we use fuel cell performance data to understand the impact of the ionomer overlayer on the catalytic activity and air performance. Finally, we use EIS and modeling to better understand the function of the ionomer overlayer.

3.1. GDE and ionomer overlayer properties

As a first step, we examined the surface of the catalyst layer and ionomer overlayer using several techniques to understand how varying the overlayer loading changed the surface. First, scanning electron microscopy (SEM) was used to image the top surface of bare and overcoated GDEs (Fig. 1). The bare GDE in Fig. 1a appears to have a rough surface. At an overlayer loading of 0.023 mg/cm^2 ionomer in Fig. 1b, the surface is noticeably smoother. With 0.045 and 0.068 mg/cm^2 ionomer in Fig. 2c and d, there appears to be additional smoothing of the surface.

To further characterize the surface roughness, we used atomic force microscopy (AFM) and stylus profilometry. These two techniques provide complimentary information at different scales. AFM provides roughness information at the nanometer scale, whereas stylus profilometry provides information roughness information at the micrometer scale. The AFM images of a bare GDE and those with and ionomer overlayer are provided in Fig. S1 of the supplementary information. The root-mean-square (RMS) roughness ($R_{RMS,AFM}$) of these images are reported in Table 1. The RMS roughness measured by stylus profilometry ($R_{RMS,SP}$) are also reported in Table 1.

The AFM measurements confirm the visual observations of the SEM images in Fig. 1. Without an ionomer overlayer, $R_{RMS,AFM}$ was 168 nm. This roughness is likely due to the carbon black support primary particle size, which TEM has shown to be 20–100 nm [34]. The primary aggregate size of a few hundred nm is also likely a component of this roughness. With an ionomer overlayer loading of 0.023 mg$_{Naf}$/cm^2, $R_{RMS,AFM}$ decreases to 111 nm. The SEM image in Fig. 1b, indicated that at this loading the ionomer overlayer is a continuous film, but the AFM measurements suggest that it is does not significantly smooth the surface and there is a large influence from the underlying catalyst layer. With additional ionomer, at a loading of 0.045 mg$_{Naf}$/cm^2, $R_{RMS,AFM}$ decreases significantly to 11.2 nm. Further addition of ionomer to 0.068 mg$_{Naf}$/cm^2 leads to a modest increase in $R_{RMS,AFM}$. These measurements show that at the nanoscale, 0.045 mg$_{Naf}$/cm^2 is needed to significantly smooth the surface.

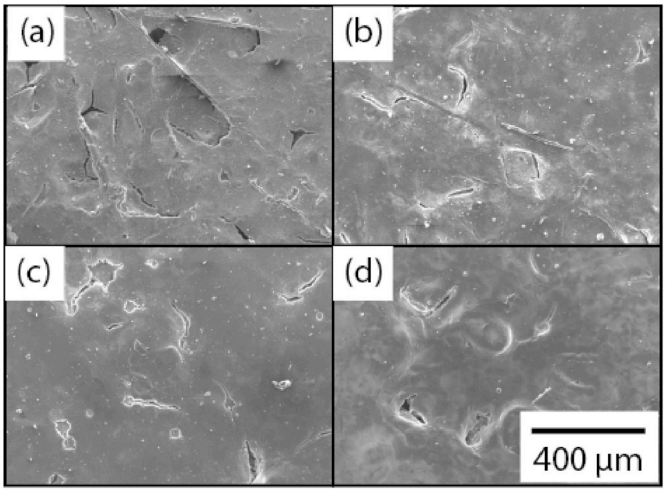

Fig. 1. Top-down scanning electron microscopy images of 0.1 mg$_{Pt}$/cm^2 CCMDs with different ionomer overlayer loadings: (a) 0 mg/cm^2, (b) 0.023 mg/cm^2, (c) 0.045 mg/cm^2, (d) 0.068 mg/cm^2.

In contrast to AFM, stylus profilometry shows that the ionomer overlayer does not change the surface roughness at the micrometer scale, when measured laterally over several millimeters. At this scale, the roughness is due to variations in the thickness of the diffusion media, likely from the carbon fibers or variations in the MPL. Assuming a density of 2 g/cm^3, the approximate ionomer overlayer thickness should be between 115 and 340 nm (depending on the loading), which is not enough to smooth out the roughness above 10 µm.

We also used cross-sectional SEM of tested MEAs to visualize interactions between the GDE and membrane. In these images the cathode GDE is located above the membrane. We were not able to cross-section and image the MEAs lacking both an overlayer and hot pressing because the diffusion media delaminated from the membrane after testing and disassembly of the test hardware. However, this is valuable information as it indicates a very poor interface between the GDE and the membrane. The images of the MEAs with 0.1 mg$_{Pt}$/cm^2 catalyst loading are shown in Fig. 2, where the catalyst layers appear brighter than lighter elements in the backscattered electron images. The MEA without an overlayer but with hot pressing is shown in Fig. 2a. There are regions where the membrane has adhered to the catalyst layer but there are also clearly large regions where the membrane does not contact the catalyst layer. The MEA with 0.045 mg$_{Naf}$/cm^2 overlayer without hot pressing, in Fig. 2b, looks similar. Sung et al. [10] suggested the role of the ionomer overlayer was to "glue" the catalyst layer to the membrane, even in the absence of hot pressing, but this image indicates that the ionomer overlayer layer alone does not provide this function, which likely explains why their GDE-based MEAs had lower performance than their CCM-based MEAs. In contrast, all of the MEAs prepared with an overlayer and hot pressing, shown in Fig. 2c–e, show that the membrane is completely laminated to the cathode catalyst layer. This indicates that both an ionomer overlayer and hot pressing are needed to adhere the catalyst layer to the membrane and maximize the interfacial contact area. Interestingly, we observe large gaps between the anode CCM catalyst layer and the anode MPL indicating hot pressing does not adhere the MPL to CCM-type catalyst layers.

Fig. 2f shows a transmission electron microscope (TEM) image of a GDE with 0.045 mg$_{Naf}$/cm^2 overlayer. Clearly visible are the catalyst layer and the ionomer overlayer. It can be seen that the ionomer overlayer is a distinct layer on top of the catalyst layer. That said, it is in full contact with the underlying catalyst layer. This should provide direct pathway for protons from the membrane to the catalyst sites when this overlayer bonds the membrane to the GDE as is indicated in the SEM images in Fig. 2.

3.2. Fuel cell testing

To better understand how the overlayer impacts MEA performance, we tested MEAs containing cathodes different ionomer overlayer loadings (0, 0.023, 0.045, and 0.068 mg$_{Naf}$/cm^2). For cathodes overlayer loadings of 0 and 0.045 mg$_{Naf}$/cm^2, MEAs were tested with and without hot pressing. For all other MEAs, the GDE was hot pressed to the membrane prior to testing. Hot-pressed CCM MEAs were prepared as a control. All of the data reported here was measured following a voltage cycling break-in procedure and three cycles of holding the MEA at 0.l V for 2 h followed by oxygen and air polarization curves. The results reported are from the polarization curves measured following the third voltage hold [30].

The measurements of catalytic performance are shown in Fig. 3. The average electrochemical surface area (ECSA) with standard deviation for the MEAs is reported in Fig. 3a. Only without both an overlayer and hot pressing was there an impact on ECSA. Otherwise, for all other combinations of Pt loading, overlayer loading, and hot pressing the ECSA was statistically the same. It was also equal to that of a hot-pressed CCM control. We believe the low ECSA of the GDE without both an ionomer overlayer hot pressing is due to a very poor interface between the

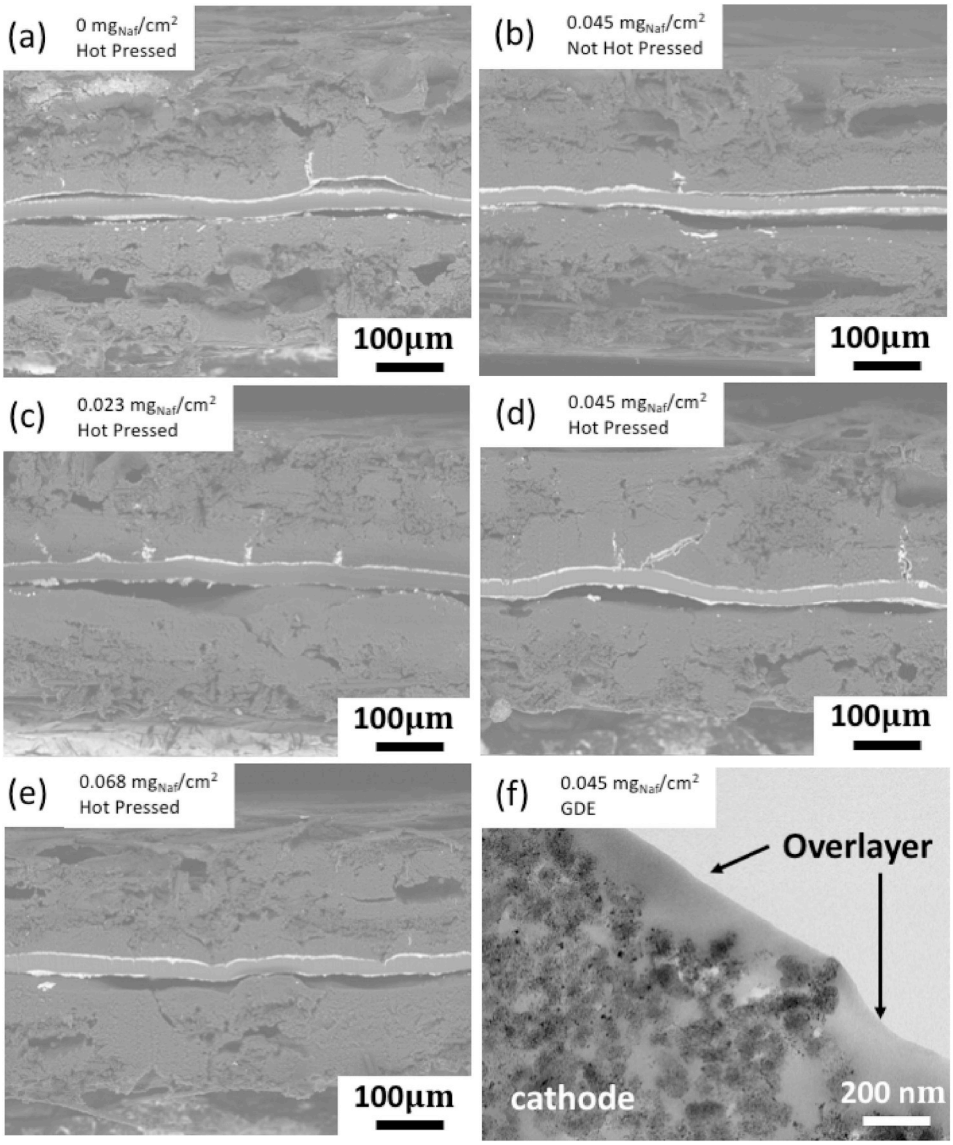

Fig. 2. Scanning electron micrographs of cross sections of tested MEAs with varying ionomer overlayer loadings and with and without hot pressing. (a) No overlayer, hot pressed; (b) 0.045 mg_{Naf}/cm^2, with hot pressing; (c) 0.023 mg_{Naf}/cm^2, with hot pressing; (d) 0.045 mg_{Naf}/cm^2, without hot pressing, (e) 0.068 mg_{Naf}/cm^2, with hot pressing. (f) TEM image of a GDE with 0.045 mg_{Naf}/cm^2. The MEAs in (a-e) are oriented with the cathode above the membrane and the anode on the bottom.

Table 1
RMS surface roughness measured by atomic force microscopy (AFM) and stylus profilometry of 0.1 mg_{Pt}/cm^2 GDEs with different Nafion overlayer loadings.

Ionomer Overlayer Loading (mg/cm^2)	AFM RMS Roughness (nm)	Stylus Profilometer RMS Roughness (µm)
0	168	15.8
0.023	111	12.4
0.045	11	16.6
0.068	32	14.4

catalyst layer and the membrane. When this MEA was removed from the cell hardware following testing the GDE did not stick to the membrane like it did for all other samples.

The average oxygen-reduction reaction mass activities measured at 0.9 V ($i_m^{0.9V}$, HFR-free, H_2 crossover corrected) are shown in Fig. 3b. To aid in understanding the statistical significance of our results, this chart also includes the average with standard deviation of $i_m^{0.9V}$ (grey solid and dashed lines, respectively) for a larger set of CCM MEAs prepared and tested at NREL in a separate study, where $i_m^{0.9V} = 427 \pm 36$ mA/mg_{Pt} [30]. The CCM MEAs prepared for this study resulted in $i_m^{0.9V\ consistent}$ with those from the previous study. Consistent with the ECSA measurements, the MEAs without an overspray and hot pressing had very low $i_m^{0.9V}$. The addition of hot pressing the GDEs (without the ionomer overlayer) to the membrane increases $i_m^{0.9}$ but it is still significantly lower than the CCM average or control CCMs tested in this study.

The addition of the ionomer overlayer significantly improved $i_m^{0.9V}$, both with and without hot pressing. With 0.023 mg_{Naf}/cm^2 and hot pressing the average $i_m^{0.9V}$ is 358 ± 33 mA/mg_{Pt}, which is just below the $i_m^{0.9V}$ range for CCMs. With a Nafion overlayer loading of 0.045 mg_{Naf}/cm^2 and no hot pressing, $i_m^{0.9V} = 349 \pm 16$ mA/mg_{Pt}. This result is consistent with the results of Sung et al. [10], which showed that ionomer overlayer GDEs without hot pressing are inferior to CCMs. With hot pressing, the average $i_m^{0.9V}$ increases to 372 ± 13 mA/mg_{Pt}, which is just below error bars of the $i_m^{0.9V}$ range for CCMs. This demonstrated the necessity of including a hot-pressing step in the preparation of GDE-type MEAs in addition to adding the ionomer overlayer. Increasing the overlayer loading to 0.068 mg_{Naf}/cm^2 resulted in $i_m^{0.9V} = 396 \pm 30$ mA/mg_{Pt}, which is now within the range variation for CCMs. Thus, from a catalyst activity perspective, there does seem to be small advantage to

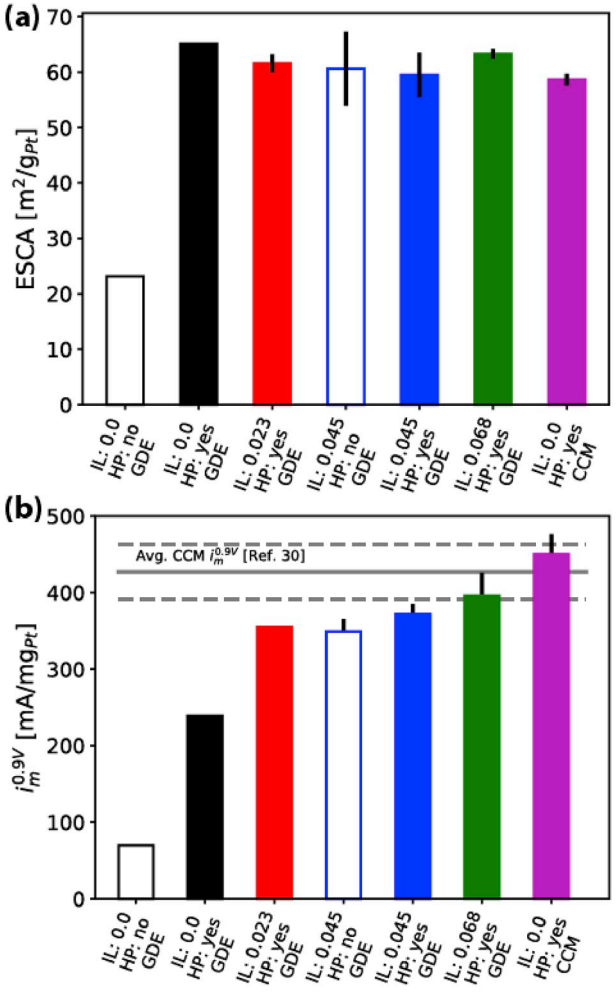

Fig. 3. Catalytic properties of MEAs with varying cathode Pt loading and ionomer overlayer loading. (a) Average electrochemical surface area (ECSA) calculated from hydrogen underpotential deposition. (b) Average cathode ORR mass activity at 0.9 V in oxygen at 80 °C, 100 %RH, 150 kPa. Current was H_2-crossover corrected. Cell potential was high-frequency resistance corrected. The polarization curve was recorded in an anodic sweep direction.

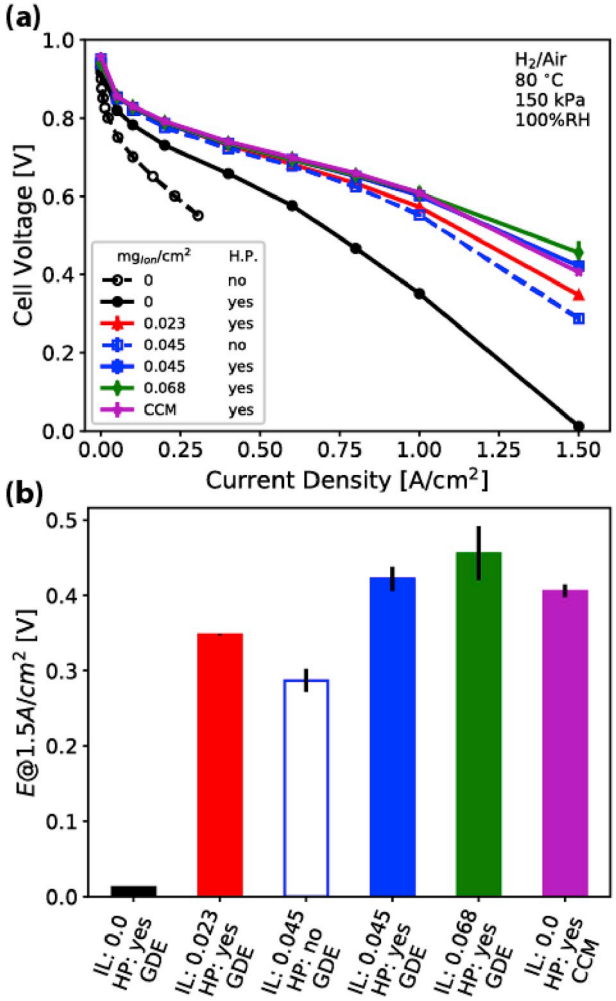

Fig. 4. Fuel cell air performance data of the MEAs with 0.1 mg_{Pt}/cm^2loading and differing loading of ionomer overlayer. (a) Air polarization curves recorded in current-control mode at 80 °C, 100% RH, 150 kPa_{abs}. Polarization curves were measured with an anodic sweep direction. (b) Bar chart of the measured cell potential at 1.5 A/cm^2. IL indicates ionomer overlayer loading in mg_{Naf}/cm^2 and HP denotes whether or not the MEA was hot pressed.

increasing the Nafion overlayer loading beyond 0.045 mg_{Naf}/cm^2 to 0.068 mg_{Naf}/cm^2. However, from the previous larger study of CCMs the standard deviation was 36 mA/mg_{Pt} so the difference in $i_m^{0.9V}$ between 0.045 mg_{Naf}/cm^2 and 0.068 mg_{Naf}/cm^2 may not be significant.

As we observed in the cross-sectional SEM images in Fig. 2, the ionomer overlayer and hot pressing results in a better interface between the catalyst layer and the membrane, which gives rise to the improvement in $i_m^{0.9V}$. The smaller variations in $i_m^{0.9V}$ between the hot pressed GDEs with different amounts of ionomer overlayer may be related to the difference in nanoscale roughness measured by AFM. Even though all overlayer loadings resulted in complete adhesion between the membrane and the catalyst layer that does not necessarily mean there is complete contact between the membrane and catalyst layer. Decreasing the nanoscale roughness could result in a modest increase in the contact area and be responsible for the slight increases in $i_m^{0.9V}$ that were measured with increasing ionomer overlayer loading.

Measurements of fuel cell performance in air for MEAs (Fig. 4a) show similar trends to the kinetic results and more clearly illustrate the effects of the overlayer and hot pressing. It is seen that not including an overlayer results in poor performance, as expected. Comparing the polarization curves for the GDEs with an overlayer and hot pressing we observed that they begin to diverge around 0.5 A/cm^2. Since these catalyst layers have the same catalyst, ionomer content, and were coated using the same method, we would not expect there to be any morphological differences that would lead to any differences in electrode oxygen transport. The electrode roughness factor at this loading and ECSA is also high enough that we would not expect non-Fickian transport losses to be significant [35]. Thus these differences in the polarization curves are likely due to differences in Ohmic losses. From the SEM images in Fig. 2, it was observed that the ionomer overlayer and hot pressing increases the interfacial contact area between the catalyst layer and the membrane. This suggests that a poor catalyst layer-membrane interface creates an interfacial resistance that increases the Ohmic losses in the MEA.

Focusing on the high-current-density region of the polarization curves most clearly demonstrates the benefit of the hot-pressing step. Fig. 4b shows the cell potential at 1.5 A/cm^2 ($E^{1.5\ A/cm2}$) for the GDE MEAs and the hot pressed CCM controls. The GDE MEAs without an overlayer and hot pressing are not included in this chart because the cells did not function at such high current densities. The hot-pressed CCM controls resulted in $E^{1.5\ A/cm2} = 406 \pm 8$ mV. An overlayer loading of 0.023 mg_{Naf}/cm^2 resulted in a lower $E^{1.5\ A/cm2}$ (348 ± 1 mV). Comparing the MEAs with 0.045 mg_{Naf}/cm^2 with and without hot pressing, we found that hot pressing increased $E^{1.5\ A/cm2}$ by 135 mV from 287 ± 15 mV to 422 ± 16 mV. This very clearly demonstrates the

importance of hot pressing. An overlayer loading 0.068 mg_{Naf}/cm^2 resulted in $E^{1.5\ A/cm2} = 456 \pm 36$ mV, which, like $i_m^{0.9V}$, is marginally larger than for 0.045 mg_{Naf}/cm^2. We also observe that 0.045 mg_{Naf}/cm^2 and 0.068 mg_{Naf}/cm^2 with hot pressing produced a slightly higher $E^{1.5\ A/cm2}$ than the hot-pressed CCM MEAs ($E^{1.5\ A/cm2} = 406 \pm 8$ mV). This is consistent to what was observed by Fultz and Chuang [14].

The air polarization curve results lead to similar conclusions as the kinetic data. Clearly, the ionomer overlayer improves cell performance. We also observe an additional benefit from hot pressing the GDEs to the membrane. As was observed from comparing $i_m^{0.9V}$, 0.023 mg_{Naf}/cm^2 was insufficient for maximum fuel cell performance. An ionomer loading of 0.068 mg_{Naf}/cm^2 resulted in a minor improvement in high-current density performance compared to 0.045 mg_{Naf}/cm^2 but given the overlapping error bars of the means we cannot conclusively say there is a benefit to additional ionomer beyond 0.045 mg_{Naf}/cm^2. Interestingly, these ionomer overlayer loadings are much lower than has been reported previously. Sung et al. [10] found their GDE-based MEAs achieved maximum power production at an overlayer loading of 0.3 mg_{Naf}/cm^2 with inferior performance at higher and lower overlayer loadings. In that study the authors did not hot press their GDEs to the membrane, which our results show is critical for maximum performance. We hypothesize, that much higher ionomer loadings may have been needed in their MEAs to compensate for the sub-optimal catalyst layer – membrane interface that exists without hot pressing, as shown in Fig. 2b.

The cross-sectional SEM images of the GDE MEAs with ionomer overlayers and hot pressing show that all ionomer overlayer loadings result in the GDE adhering to the membrane and thus cannot explain the differences in performance between the MEAs with different ionomer overlayer loadings. Instead the difference seems to be explained by the nanoscale roughness of the ionomer-overcoated GDE surface. As reported in Table 1, AFM showed that an overlayer loading of 0.023 mg_{Naf}/cm^2 reduced $R_{RMS,AFM}$ from 168 nm without an overlayer to 111 nm. Overlayer loadings of 0.045 and 0.068 mg_{Naf}/cm^2 further reduced the roughness to 11.2 and 32.5 nm, respectively. This difference appears to be significant enough to impact the performance. While an overlayer loading of 0.023 mg_{Naf}/cm^2 effectively adheres the GDE to the membrane, due to the nanoscale roughness of the GDE there may be areas on the nanoscale where the GDE does not contact the membrane, resulting in less than 100% contact area between the GDE and membrane. When the ionomer overlayer loading is increased, causing $R_{RMS,AFM}$ to decrease, the contact area between the GDE and the membrane is also increased. The decreased contact area for 0.023 mg_{Naf}/cm^2 overlayer loading would likely manifest itself as an increased interfacial resistance because the protons would be conducted through a restricted area.

3.3. Electrochemical impedance spectroscopy

Based on the air polarization curves we suspected that the improved catalyst layer-membrane interface, due to the ionomer overlayer and hot pressing, improved proton conduction and reduced resistive losses in the MEAs. To better understand the resistances in the MEAs we utilized H_2/N_2 EIS and modeling to quantify the different cell resistances, specifically the HFR and the cathode bulk catalyst layer protonic resistance of (R_{CL}). Initially, we attempted a simple analysis of estimating the HFR by interpolating the value of the real impedance (Z') where the imaginary impedance (Z'') was zero and estimated (R_{CL}) by measuring the length of the 45° region of the Nyquist plot, as described by Thompson and Baker [36]. We found that the latter part of this method did not produce reasonable results due to difficulty defining the length of 45° region.

We then fit these data using a one-dimensional physics-based impedance model developed by Setzler and Fuller [37], which produced much more consistent results.

A plot of one measured impedance spectrum with the modeled fit is shown in Fig. 5. For this spectrum the model clearly represents the data well. The values of the fit parameters and residual error for all of the

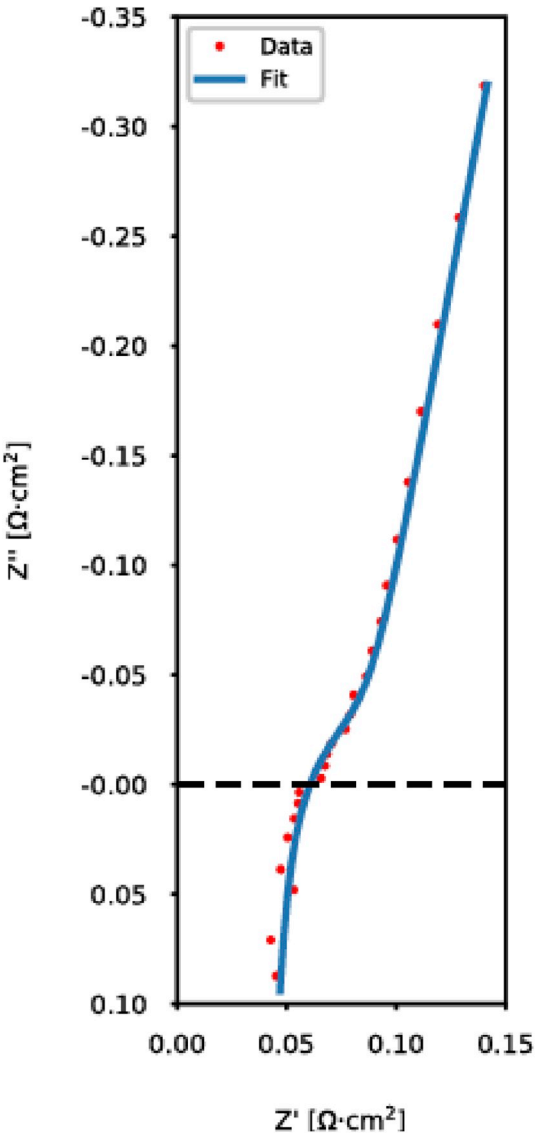

Fig. 5. Exemplary measured H_2/N_2 EIS spectrum (red) with model fit (blue). (For interpretation of the references to color in this figure legend, the reader is referred to the Web version of this article.)

MEAs are reported in Table S1 of the supplementary information with plots of selected fit parameters shown in Fig. 6. L_{wire} is consistent across all samples, as expected, because the same hardware and test equipment were used for all measurements. For the CCM MEAs it can be seen that the standard errors were less than 15% of the fitted value indicating good agreement between the measured data and the model. The values for R_Ω are shown in Fig. 6a. For a 25 μm Nafion membrane used here, the average fitted value of 36 mΩ-cm^2 is close to the expected value (approx. 40 mΩ-cm^2) based on membrane protonic and cell electronic resistances reported by Makharia et al., further validating the applicability of the model [26].These MEAs also had an average φ of 0.94 (shown in Fig. 6b), which also indicates consistency between the measured data and the model. While φ in this model, $0 \leq \varphi \leq 1$, has many interpretations in the literature, it is commonly accepted that a value of less than one is a result of a distribution of resistive-capacitive (RC) time constants on or in the electrode. [38] It has been shown that a distribution of current density can give rise to $\varphi < 1$ [39]. A distribution in current density across an otherwise ideal catalyst layer and membrane could be the result from uneven contact between them. That is to say, lower values of φ indicate non-ideal MEA behavior likely due to a

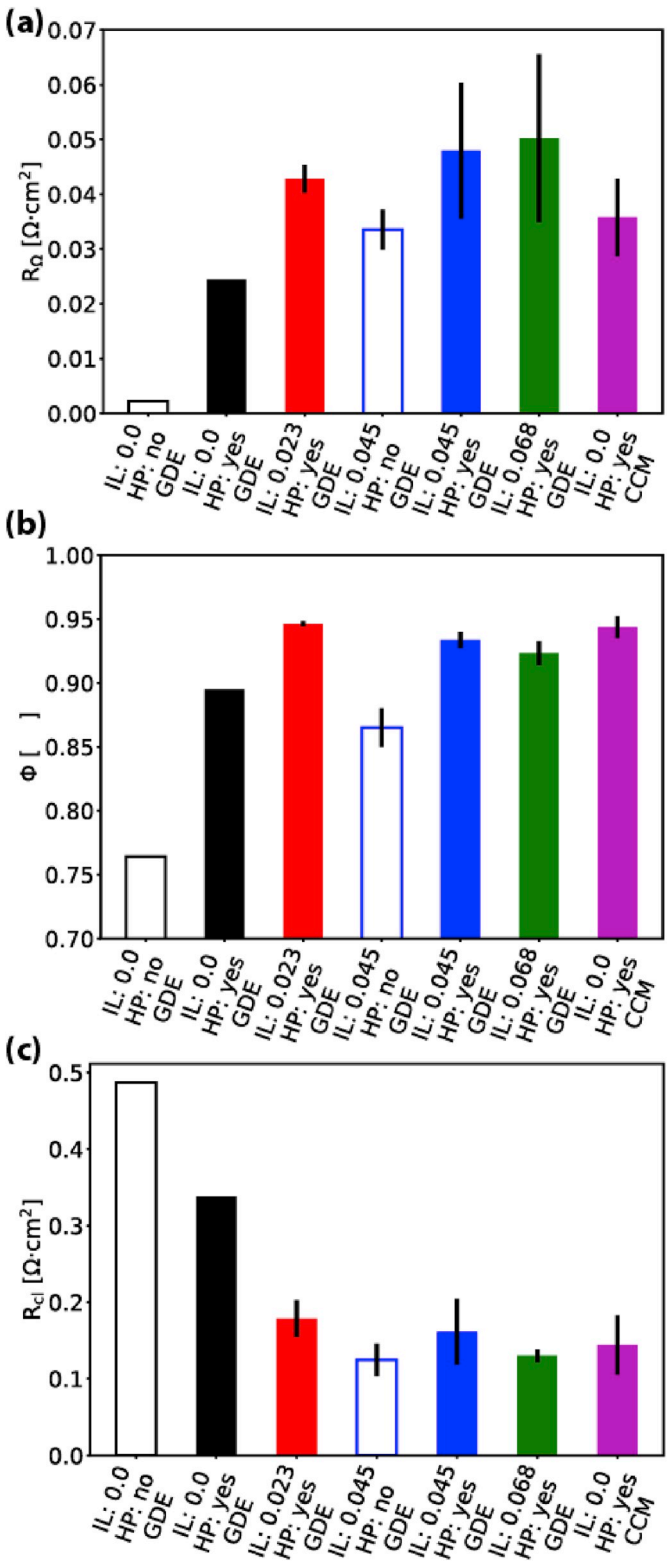

Fig. 6. Bar charts of several fit parameters from the model fit of the EIS measurements. (a) Membrane resistance (R_Ω), (b) constant phase element exponent (φ), and (c) catalyst layer resistance (R_{CL}). IL indicates ionomer overlayer loading in mg_{Naf}/cm^2 and HP denotes whether or not the MEA was hot pressed.

distribution of current density and RC time constants across the catalyst layer – membrane interface. For the CCMs, which have a good catalyst layer – membrane interface, the current distribution should be homogenous due to the close to 100% contact between the catalyst layer and the membrane.

In contrast to the CCM MEAs, for the GDE MEAs without an overlayer or hot pressing the fit parameters for these had larger standard errors than hot pressed MEAs with an overlayer and in some cases, values that are non-physical, specifically R_Ω of only a 2.3 mΩ-cm^2 for the MEAs without an overlayer or hot pressing. These MEAs also had $\varphi < 0.9$ indicating a non-uniform current distribution, likely due to the poor catalyst layer – membrane interface. Based on what was observed in Fig. 2 this makes physical sense. Looking at Fig. 2a and b there are areas where the catalyst layer does not contact the membrane and other areas where it does. Therefore, all of the protons entering the catalyst layer from the membrane would be required to pass through the catalyst layer – membrane contact points, resulting in very high local current density, whereas the locations of catalyst layer disconnected would have very low local current density. This would give rise to the non-uniform current distribution indicated by low φ. We do see some dependence of φ on GDE assembly conditions. Adding an ionomer overlayer (without hot pressing) or hot pressing (without an ionomer layer) increased φ compared to the MEA without both an ionomer overlayer and hot pressing, indicating an increase in uniformity of the current density due to increased contact area between the catalyst layer and membrane, which is consistent the observed increase in fuel cell performance with the addition of an ionomer overlayer or hot pressing.

For all of the MEAs with both an ionomer overlayer and hot pressing, the agreement between the model and the measured spectra was good and $\varphi > 0.9$ indicating close to ideal behavior. Consistent with the fuel cell performance data in Fig. 4. Referring back to Fig. 2, the MEAs with an ionomer overlayer and hot pressing were bonded to the membrane which would result in a close to homogenous current distribution and result in φ close to 1, similar to what was observed in the CCM MEAs. With an overlayer and hot pressing we do not observe a dependence of the ionomer overlayer loading on R_Ω. We would not expect to see differences in R_Ω between samples because all of the MEAs used the same membrane material and cell hardware.

The fit parameter that showed the most dependence on fabrication conditions was the catalyst layer proton resistance, R_{CL}, shown in Fig. 6c. Here we observed a clear trend with ionomer overlayer loading and hot pressing. The MEAs with highest R_{CL} (without an overlayer or hot pressing) had regions where the catalyst layer did not contact the membrane. In these cases, protons would have to enter the catalyst layer in one of the regions where the membrane contacts the catalyst layer and then travel laterally to reach the regions catalyst layer not in contact the membrane. This more tortuous path results in results in a higher measured resistance. Comparing the MEAs without an overlayer, hot pressing decreases R_{CL}. Adding an ionomer overlayer further decreases R_{CL}. Comparing only the MEAs with the ionomer overlayer, we observe that additional ionomer results in a slight decrease in R_{CL}. With an overlayer loading of 0.023 mg_{Naf}/cm^2 it is observed that the value of R_{CL} is slightly higher than that of the CCM MEAs. Increasing the loading to 0.045 mg_{Naf}/cm^2 with hot pressing further decreases R_{CL} to a value close to that of the CCM MEAs. This is consistent with the observed air fuel cell performance, where an overlayer loading of 0.023 mg_{Naf}/cm^2 appeared to have higher Ohmic losses than 0.045 mg_{Naf}/cm^2. Increasing the ionomer overlayer loading to 0.068 mg_{Naf}/cm^2 results in an additional, but small, decrease in R_{CL}. It is also found that for ionomer overlayer loadings of 0.045 mg_{Naf}/cm^2 and 0.068 mg_{Naf}/cm^2 with hot pressing R_{CL} is similar to that of the hot-pressed CCM control MEAs. This is consistent with MEA performance as at these ionomer loadings the GDE MEAs had similar $i_m^{0.9V}$ and $E^{1.5\ A/cm2}$ to the hot-pressed CCM MEAs. The lowest R_{CL} was for the MEAs with 0.045 mg_{Naf}/cm^2 without hot pressing. However, for these MEAs φ is relatively low and parameter standard errors are relatively high, so the model may not be accurately representing the physics here, resulting in an inaccurate value of R_{CL}.

To validate our hypothesis that variations in air performance were a function of proton conductivity, we compared measured fuel cell parameters with model-determined values of R_{CL}. Fig. 7a compares the cell

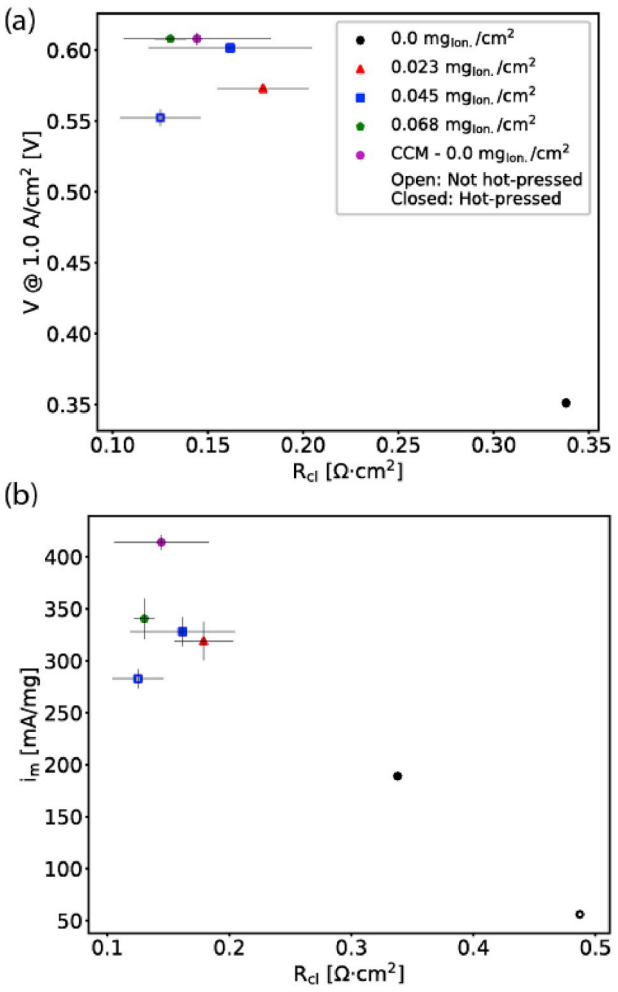

Fig. 7. Correlation between R_{CL} and fuel cell performance metrics. (a) Cell potential at 1.0 A/cm^2 measured in H_2/air and (b) ORR mass activity at 0.9 V. Color indicates catalyst layer loading and marker shape indicates ionomer overlayer loading. Filled symbols – hot pressed MEAs. Unfilled symbols – not hot pressed MEAs.

potential at 1.0 A/cm^2 ($E^{1.0\ A/cm2}$) to R_{CL}. We see a clear correlation that $E^{1.0\ A/cm2}$ increases as R_{CL} decreases. As was discussed in the previous section, it was observed that the polarization curves diverged around 0.5 A/cm^2, which we attributed to differences in Ohmic resistance losses. These results confirm this attribution, as we clearly see that a sub-optimal catalyst layer – membrane interface leads to increased R_{CL}, which would increase Ohmic losses and decrease fuel cell performance.

Additionally, Fig. 7b shows the dependence of $i_m^{0.9V}$ on R_{CL}. Previous analysis of catalyst layer resistance has shown that a high R_{CL} leads to protons reacting closer to the membrane [25,33]. If this resistance is large enough it would lead to only a fraction of the catalyst layer being utilized, which would result in a reduced $i_m^{0.9V}$. This is exactly what we observe with $i_m^{0.9V}$ increasing with decreasing R_{CL}. As shown in the cross-sectional SEM images in Fig. 2, the MEAs with highest R_{CL} (without an overlayer or hot pressing) had regions where the catalyst layer did not contact the membrane. In these cases, protons would have to enter the catalyst layer in one of the regions where the membrane contacts the catalyst layer and then travel laterally to reach the regions catalyst layer not in contact the membrane. This more tortuous path results in the protons reacting closer to the membrane instead of through the full thickness of the catalyst layer. In contrast, when the catalyst layer – membrane interface is complete, protons have a low tortuosity pathway and do not have to travel laterally to reach catalyst sites, which results in high catalyst utilization as indicated by the high $i_m^{0.9V}$ values.

4. Conclusion

This work presents a parametric study of the influence of an ionomer overlayer and hot pressing on fuel cell performance in spray-coated GDE-based MEAs. We have shown that both an ionomer overlayer and hot pressing of the GDE to the membrane are required for best fuel cell performance. We observed that the overlayer provides two functions: adhering the GDE to the membrane and smoothing the GDE surface to provide more contact area between the catalyst layer and the membrane. These two functions reduce the Ohmic losses, which leads to improved catalyst utilization and fuel cell performance. Through our modeling of EIS data, we observed that there is a critical ionomer overlayer loading needed to obtain similar catalyst layer resistance to CCM-based MEAs. The results presented also provide insights that are likely relevant for the optimization of GDEs prepared using roll-to-roll or other coating methods.

Declaration of competing interest

The authors declare that they have no known competing financial interests or personal relationships that could have appeared to influence the work reported in this paper.

Acknowledgments

This work was authored in part by Alliance for Sustainable Energy, LLC, the manager and operator of the National Renewable Energy Laboratory for the U.S. Department of Energy (DOE) under Contract No. DE-AC36-08GO28308. Funding provided by U.S. Department of Energy Office of Energy Efficiency and Renewable Energy Advanced Manufacturing Office, technology manager David Hardy. The views expressed in the article do not necessarily represent the views of the DOE or the U.S. Government. The U.S. Government retains and the publisher, by accepting the article for publication, acknowledges that the U.S. Government retains a nonexclusive, paid-up, irrevocable, worldwide license to publish or reproduce the published form of this work, or allow others to do so, for U.S. Government purposes. The authors would like to thank Adam Phillips for insight related to the ionomer overlayer and hot-pressing procedure.

Appendix A. Supplementary data

Supplementary data to this article can be found online at Mhttps://doi.org/10.1016/j.jpowsour.2019.227581.

References

[1] S. Kim, M. Khandelwal, C. Chacko, M.M. Mench, Investigation of the impact of interfacial delamination on polymer electrolyte fuel cell performance, J. Electrochem. Soc. 156 (2009) B99–B108, https://doi.org/10.1016/j.elecom.2007.10.029.
[2] J.-H. Kim, H.Y. Ha, I.-H. Oh, S.-A. Hong, H.-I. Lee, Influence of the solvent in anode catalyst ink on the performance of a direct methanol fuel cell, J. Power Sources 135 (2004) 29–35, https://doi.org/10.1016/j.jpowsour.2004.03.058.
[3] K. Kadowaki, Y. Tabe, T. Chikahisa, Role of micro-porous layer for water transfer phenomena in PEFC, ECS Trans. 41 (2011) 431–438, https://doi.org/10.1149/1.3635577.
[4] S.J. Shin, J.K. Lee, H.Y. Ha, S.A. Hong, H.S. Chun, Effect of the catalytic ink preparation method on the performance of polymer electrolyte membrane fuel cells, J. Power Sources 106 (2002) 146–152.
[5] C.M. Johnston, K.-S. Lee, T. Rockward, A. Labouriau, N. Mack, Y.S. Kim, Impact of solvent on ionomer structure and fuel cell durability, ECS Trans. 25 (2009) 1617–1622.
[6] Y. Liu, M.W. Murphy, D.R. Baker, W. Gu, C. Ji, J. Jorne, et al., Proton conduction and oxygen reduction kinetics in PEM fuel cell cathodes: effects of ionomer-to-carbon ratio and relative humidity, J. Electrochem. Soc. 156 (2009) B970, https://doi.org/10.1021/jp048985k.
[7] T.-H. Yang, Y.-G. Yoon, G.-G. Park, W.-Y. Lee, C.-S. Kim, Fabrication of a thin catalyst layer using organic solvents, J. Power Sources 127 (2004) 230–233, https://doi.org/10.1016/j.jpowsour.2003.09.018.

[8] S.G. Yan, B. Sompalli, J.C. Doyle, Durable Membrane Electrode Assembly Catalyst Coated Diffusion Media with No Lamination to Membrane, 2007. U.S. Patent Office. 7291419B2.
[9] T. Kusano, T. Hiroi, K. Amemiya, M. Ando, T. Takahashi, M. Shibayama, Structural evolution of a catalyst ink for fuel cells during the drying process investigated by CV-SANS, Polym. J. 47 (2015) 546–555, https://doi.org/10.1038/pj.2015.36.
[10] C.-C. Sung, C.-Y. Liu, C.C.J. Cheng, Performance improvement by a glue-functioned Nafion layer coating on gas diffusion electrodes in PEM fuel cells, Int. J. Hydrogen Energy 39 (2014) 11700–11705, https://doi.org/10.1016/j.ijhydene.2014.05.110.
[11] J.-C. Lin, C.-M. Lai, F.-P. Ting, S.-D. Chyou, K.-L. Hsueh, Influence of hot-pressing temperature on the performance of PEMFC and catalytic activity, J. Appl. Electrochem. 39 (2009) 1067–1073, https://doi.org/10.1007/s10800-008-9758-1.
[12] S.-J. Seo, J.-J. Woo, S.-H. Yun, H.-J. Lee, J.-S. Park, T. Xu, et al., Analyses of interfacial resistances in a membrane-electrode assembly for a proton exchange membrane fuel cell using symmetrical impedance spectroscopy, Phys. Chem. Chem. Phys. 12 (2010) 15291, https://doi.org/10.1039/B611690F.
[13] M. Prasanna, H.Y. Ha, E.A. Cho, S.A. Hong, I.H. Oh, Investigation of oxygen gain in polymer electrolyte membrane fuel cells, J. Power Sources 137 (2004) 1–8, https://doi.org/10.1016/j.jpowsour.2004.05.034.
[14] D.W. Fultz, P.-Y.A. Chuang, The property and performance differences between catalyst coated membrane and catalyst coated diffusion media, J. Fuel Cell Sci. Technol. 8 (2011), 041010, https://doi.org/10.1115/1.4003632.
[15] M. Breitwieser, M. Klingele, B. Britton, S. Holdcroft, Improved Pt-utilization efficiency of low Pt-loading PEM fuel cell electrodes using direct membrane deposition, Electrochem. Commun. 60 (2015) 168–171, https://doi.org/10.1016/j.elecom.2015.09.006.
[16] M. Klingele, M. Breitwieser, R. Zengerle, S. Thiele, Direct deposition of proton exchange membranes enabling high performance hydrogen fuel cells, J. Mater. Chem. A. 3 (2015) 11239–11245, https://doi.org/10.1039/C5TA01341K.
[17] S. Vierrath, M. Breitwieser, M. Klingele, B. Britton, S. Holdcroft, R. Zengerle, et al., The reasons for the high power density of fuel cells fabricated with directly deposited membranes, J. Power Sources 326 (2016) 170–175, https://doi.org/10.1016/j.jpowsour.2016.06.132.
[18] M. Klingele, B. Britton, M. Breitwieser, S. Vierrath, A completely spray-coated membrane electrode assembly, Electrochem. Commun. 70 (2016) 65–68, https://doi.org/10.1016/j.elecom.2016.06.017.
[19] X. Ding, S. Didari, T.F. Fuller, T.A.L. Harris, Membrane electrode assembly fabrication process for directly coating catalyzed gas diffusion layers, J. Electrochem. Soc. 159 (2012) B746, https://doi.org/10.1149/2.103206jes.
[20] M. Prasanna, E.A. Cho, T.H. Lim, I.H. Oh, Effects of MEA fabrication method on durability of polymer electrolyte membrane fuel cells, Electrochim. Acta 53 (2008) 5434–5441, https://doi.org/10.1016/j.electacta.2008.02.068.
[21] M.B. Sassin, Y. Garsany, B.D. Gould, K.E. Swider-Lyons, Fabrication method for laboratory-scale high-performance membrane electrode assemblies for fuel cells, Anal. Chem. 89 (2016) 511–518, https://doi.org/10.1021/acs.analchem.6b03005.
[22] H. Tang, S. Wang, S.P. Jiang, M. Pan, A comparative study of CCM and hot-pressed MEAs for PEM fuel cells, J. Power Sources 170 (2007) 140–144, https://doi.org/10.1016/j.jpowsour.2007.03.062.
[23] S. Martemianov, V.A. Raileanu Ilie, C. Coutanceau, Improvement of the proton exchange membrane fuel cell performances by optimization of the hot pressing process for membrane electrode assembly, J. Solid State Electrochem. 18 (2013) 1261–1269, https://doi.org/10.1016/j.jpowsour.2009.09.051.
[24] Q. Meyer, N. Mansor, F. Iacoviello, P.L. Cullen, R. Jervis, Investigation of hot pressed polymer electrolyte fuel cell assemblies via X-ray computed tomography, Electrochim. Acta 242 (2017) 125–136, https://doi.org/10.1016/j.electacta.2017.05.028.
[25] I.V. Zenyuk, E.C. Kumbur, S. Litster, Deterministic contact mechanics model applied to electrode interfaces in polymer electrolyte fuel cells and interfacial water accumulation, J. Power Sources 241 (2013) 379–387, https://doi.org/10.1016/j.jpowsour.2013.03.165.
[26] R. Makharia, M.F. Mathias, D.R. Baker, Measurement of catalyst layer electrolyte resistance in PEFCs using electrochemical impedance spectroscopy, J. Electrochem. Soc. 152 (2005) A970, https://doi.org/10.1016/S0013-4686(98)00128-5.
[27] M. Breitwieser, M. Klingele, S. Vierrath, R. Zengerle, S. Thiele, Tailoring the membrane-electrode interface in PEM fuel cells: a review and perspective on novel engineering approaches, Adv. Energy Mater. 8 (2017) 1701257, https://doi.org/10.1002/adma.201404598.
[28] G.A.F. Seber, C.J. Wild, Nonlinear regression. https://www.wiley.com/en-us/Nonlinear+Regression-p-9780471725312, 2005.
[29] P.A. Rapaport, A.J. Blowers, L. James, B. Lakshmanan, Fast MEA Break-In and Voltage Recovery, US Patent Office, 2015, p. 9099703B2.
[30] S. Kabir, D.J. Myers, N.N. Kariuki, J. Park, G. Wang, A.M. Baker, et al., Elucidating the dynamic nature of fuel cell electrodes as a function of conditioning: an ex-situ materials characterization and in-situ electrochemical diagnostic study, ACS Appl. Mater. Interfaces 11 (2019) 45016–45030, https://doi.org/10.1021/acsami.9b11365.
J.R. Pfeilsticker, Open-source impedance fitter. https://github.com/NREL/OSIF, 2018.
[32] Pauli Virtanen, Ralf Gommers, Travis E. Oliphant, Matt Haberland, Tyler Reddy, David Cournapeau, Evgeni Burovski, Pearu Peterson, Warren Weckesser, Jonathan Bright, Stéfan J. van der Walt, Matthew Brett, Joshua Wilson, K. Jarrod Millman, Nikolay Mayorov, Andrew R. J. Nelson, Eric Jones, Robert Kern, Eric Larson, CJ Carey, İlhan Polat, Yu Feng, Eric W. Moore, Jake VanderPlas, Denis Laxalde, Josef Perktold, Robert Cimrman, Ian Henriksen, E.A. Quintero, Charles R Harris, Anne M. Archibald, Antônio H. Ribeiro, Fabian Pedregosa, Paul van Mulbregt, and SciPy 1.0 Contributors. (2019) SciPy 1.0–Fundamental Algorithms for Scientific Computing in Python. preprint arXiv:1907.10121.
[33] K.C. Neyerlin, W. Gu, J. Jorne, A. Clark, H.A. Gasteiger, Cathode catalyst utilization for the ORR in a PEMFC, J. Electrochem. Soc. 154 (2007) B279, https://doi.org/10.1016/j.jpowsour.2004.03.028.
[34] B.T. Sneed, D.A. Cullen, K.S. Reeves, O.E. Dyck, D.A. Langlois, R. Mukundan, et al., 3D analysis of fuel cell electrocatalyst degradation on alternate carbon supports, ACS Appl. Mater. Interfaces 9 (2017) 29839–29848, https://doi.org/10.1021/acsami.7b09716.
[35] A. Kongkanand, M.F. Mathias, The priority and challenge of high-power performance of low-platinum proton-exchange membrane fuel cells, J. Phys. Chem. Lett. (2016) 1127–1137, https://doi.org/10.1021/acs.jpclett.6b00216.
[36] E.L. Thompson, D. Baker, Proton conduction on ionomer-free Pt surfaces, ECS Trans. 41 (2011) 709–720, https://doi.org/10.1149/1.3635605.
[37] B.P. Setzler, T.F. Fuller, A physics-based impedance model of proton exchange membrane fuel cells exhibiting low-frequency inductive loops, J. Electrochem. Soc. 162 (2015) F519–F530, https://doi.org/10.1149/2.0361506jes.
[38] K.S. Cole, R.H. Cole, Dispersion and absorption in dielectrics I. Alternating current characteristics, J. Chem. Phys. 9 (1941) 341–351, https://doi.org/10.1063/1.1745400.
[39] J.-B. Jorcin, M.E. Orazem, N. Pébère, B. Tribollet, CPE analysis by local electrochemical impedance spectroscopy, Electrochim. Acta 51 (2006) 1473–1479, https://doi.org/10.1016/j.electacta.2005.02.128.